REPORT DOCUMENTATION PAGE

Form Approved
OMB No. 0704-0188

1. AGENCY USE ONLY (Leave blank)	2. REPORT DATE	3. REPORT TYPE AND DATES COVERED
		Preprint Dec. 1990

4. TITLE AND SUBTITLE
"A Study of Dynamic Stall Using Real Time Interferometry"

5. FUNDING NUMBERS
ARO M.PR. 11491

6. AUTHOR(S)
L. W. Carr, M. S. Chandrasekhara, S. Ahmed and N. Brock

7. PERFORMING ORGANIZATION NAME(S) AND ADDRESS(ES)
Naval Postgraduate School, Monterey, CA 93943
Navy-NASA Joint Institute of Aeronautics
NASA Ames Research Center, M. S. 260-1
Moffett Field, CA 94035

8. PERFORMING ORGANIZATION REPORT NUMBER

9. SPONSORING/MONITORING AGENCY NAME(S) AND ADDRESS(ES)
U. S. Army Research Office
P. O. Box 12211
Research Triangle Park, NC 27709-2211

10. SPONSORING/MONITORING AGENCY REPORT NUMBER
ARO 27894.3-EG

11. SUPPLEMENTARY NOTES
The view, opinions and/or findings contained in this report are those of the author(s) and should not be construed as an official Department of the Army position, policy, or decision, unless so designated by other documentation.

12a. DISTRIBUTION/AVAILABILITY STATEMENT
Approved for public release; distribution unlimited.

12b. DISTRIBUTION CODE

13. ABSTRACT *(Maximum 200 words)*

Dynamic stall over an oscillating airfoil in compressible flow was studied using a real-time interferometry technique. Instantaneous flow field data was obtained for various unsteady as well as steady flow conditions. The details of the dynamic stall vortex, including its formation and development have been revealed by the interferograms, resulting in the first documentation of the complete dynamic stall flow field under compressible flow conditions. Comparison of steady flow interferograms with those taken in unsteady flow reveal significant delay in development of leading edge suction peaks in the unsteady case. The interferograms permit detailed analysis of the leading edge pressure field; as many as 13 pressure values have been obtained around the leading edge in the first 1% of the airfoil chord. The results offer significant new insight into the character of the dynamic stall vortex, and the stall delay that is observed during dynamic motions.

14. SUBJECT TERMS	15. NUMBER OF PAGES
Unsteady Separated Flows, Dynamic Stall, Compressibility Effects, Optical Technique, Real Time Interferometry	16. PRICE CODE

17. SECURITY CLASSIFICATION OF REPORT	18. SECURITY CLASSIFICATION OF THIS PAGE	19. SECURITY CLASSIFICATION OF ABSTRACT	20. LIMITATION OF ABSTRACT
UNCLASSIFIED	UNCLASSIFIED	UNCLASSIFIED	UL

AIAA 91-0007

A Study of Dynamic Stall Using Real Time Interferometry

L.Carr, U.S.Army Aeroflightdynamics Directorate, NASA-Ames, Moffett Field, CA;

M.Chandrasekhara, Navy-NASA Joint Institute of Aeronautics, Naval Postgraduate School, Monterey, CA ;

S.Ahmed, MCAT Institute, San Jose, CA;

N.Brock, Aerometrics, Sunnyvale, CA

29th Aerospace Sciences Meeting

January 7-10, 1991/Reno, Nevada

A Study of Dynamic Stall Using Real Time Interferometry

L.W. Carr[1]
Aeroflightdynamics Directorate, U.S.Army AVSCOM
and Fluid Dynamics Research Branch
NASA Ames Research Center, Moffett Field, CA 94035

M.S. Chandrasekhara[2]
Navy-NASA Joint Institute of Aeronautics
Department of Aeronautics and Astronautics
Naval Postgraduate School, Monterey, CA 93943

S. Ahmed[3]
MCAT Institute, San Jose, CA 95127

and

N.J. Brock[4]
Aerometrics, Sunnyvale, CA 94086

Abstract

Dynamic stall over an oscillating airfoil in compressible flow was studied using a real-time interferometry technique. Instantaneous flow field data was obtained for various unsteady as well as steady flow conditions. The details of the dynamic stall vortex, including its formation and development have been revealed by the interferograms, resulting in the first documentation of the complete dynamic stall flow field under compressible flow conditions. Comparison of steady flow interferograms with those taken in unsteady flow reveal significant delay in development of leading edge suction peaks in the unsteady case. The interferograms permit detailed analysis of the leading edge pressure field; as many as as 13 pressure values have been obtained around the leading edge in the first 1% of the airfoil chord. The results offer significant new insight into the character of the dynamic stall vortex, and the stall delay that is observed during dynamic motions.

Nomenclature

C_p	pressure coefficient
c	airfoil chord
f	frequency of oscillation
k	reduced frequency = $\frac{\pi f c}{U_\infty}$
L	test section span
M	free stream Mach number
n	refractive index
n_r	refractive index at reference conditions
n_0	refractive index at atmospheric conditions
S	distance along airfoil surface
U_∞	free stream velocity
x	chordwise distance
z	spanwise distance
α	angle of attack
$\overline{\Delta PL}$	average path length difference
ϵ	fringe number
λ_0	wavelength of the laser
ρ	density
ρ_r	density at reference conditions
ρ_0	density at atmospheric conditions
ϕ	phase angle of oscillation
ω	circular frequency

1. Introduction

The control and utilization, or alleviation, of the dynamic-stall-induced aerodynamic loads which appear on helicopter rotor blades, and on rapidly moving conventional aircraft wings or control surfaces, will require a much greater understanding of the character of the unsteady flow field that occurs on these aerodynamic surfaces than is currently available. Significant study of the dynamic stall process has already been performed[1]. The effect of compressibility on dynamic stall airloads has been identified by a number of researchers[2-5]. However, experimental verification of the effects of the vortex on the compressible flow field have been limited so far to measurements on the airfoil surface[6] or qualitative imaging of the general flow field[7-9], with the exception of the work of Lee, et al[10], where much of the flow field was blocked by the system used to support the model. In the past, techniques for obtaining interferograms of compressible flows have required significant post-processing(e.g. holographic interferometry); real-time techniques such as Mach-Zender

---

1. Group Leader, Unsteady Viscous Flows, Member, AIAA

2. Assistant Director and Adjunct Research Professor, Assoc. Fellow, AIAA

3. Research Scientist, Member, AIAA. *On leave from National Aeronautical Laboratory, Bangalore, India*

4. Research Scientist

interferometry systems [11] required expensive optics, and needed massive structure to reduce sensitivity to vibration. A new technique, based on the use of vibration-insensitive real-time interferometry known as point diffraction interferometry(PDI), has now been used to obtain results that reveal new details about the development of the dynamic stall vortex, and its effect on the flow over pitching airfoils.

The complexity and rapidity of the flow development during dynamic stall as well as the large pressure gradients that form near the leading edge make quantitative measurement very challenging and difficult. Better understanding of the stall process will be needed before any alleviation of the adverse effects of the dynamic stall event can be achieved; this will require careful study of the flow during the stall inception. However, physical space limitations greatly restrict the density of sensors that can be installed in this region of the airfoil, and the presence of these sensors can actually affect the flow being studied. Thus, issues about the origin of the dynamic stall vortex, and explanation of why and how stall delay occurs have remained very difficult to address experimentally; the technique used in the present study offers new opportunities for such a study. Some of the early results showing the flow development as obtained with this new technique are discussed in the present paper.

2. Description of the Facility

The present study was performed in the Compressible Dynamic Stall Facility(CDSF) at the NASA Ames Research Center Fluid Mechanics Laboratory(FML). The CDSF is specifically designed for study of dynamic stall over a range of Mach numbers, using non-intrusive optical flow diagnostic techniques. It is operated as a part of the in-draft tunnel complex at the FML(for details, see Carr and Chandrasekhara[12]). The CDSF is specially designed so that airfoil supports do not block the view of the airfoil. The airfoil is supported between two 2.54cm thick optical quality glass windows by pins that are smaller than the local airfoil thickness; thus the airfoil can be viewed unobstructed by any support mechanism(figure 1). The window/airfoil combination is driven in sinusoidal oscillation by a 4-bar, push-rod-flywheel system, about the 25% chord position. This permits study of the flow at the leading edge, where the dynamic stall vortex forms, as well as the flow field away from the airfoil. The drive motor is a variable speed a.c. motor with a controller to maintain speed to within 1%. The drive mechanism can oscillate the airfoil at frequencies up to 100 Hz, with oscillatory amplitudes ranging from 2° - 10°. The mean angle of attack can be varied from 0° - 15°. Phase angle in the cycle is determined by an optical encoder keyed to the flywheel. The present test conditions included M= 0.2-0.45, for k = 0.0 - 0.10, Reynolds number = 400,000- 900,000, with the airfoil oscillating at $\alpha = 10° - 10°\sin\omega t$. The airfoil was NACA 0012 with a 7.62cm chord.

The interferometric images were obtained by triggering a laser light source at defined phase angles through the oscillation cycle. The light source was a pulsed Nd:YAG laser with a frequency doubler, operating at a wavelength of 532nm. The phase angle for the interferogram was chosen by setting switches on a specially designed counter circuit box. Since the laser took a finite time to actually emit light, additional electronics were incorporated in the circuitry to display the phase angle when the laser actually fired. This was accomplished by sensing the light using a photo diode; when the laser fired, the output of the photo diode was used to freeze the angle of attack display so that the precise angle at which the image was taken could be recorded.

3. Point Diffraction Interferometry Technique

3.1 Principle

The point diffraction interferometry(PDI) technique used for the present test is based on the work of Smartt[13,14] as first applied to compressible flow by Bachalo and Houser[15]. The PDI technique utilizes the ability of a point discontinuity(in the form of a pin-hole) located at the image of a point source to diffract a portion of the incident light into a spherical reference wave front. In the Smartt interferometer, the light passing through the flow is used to produce the reference wave, by placing a sheet of partially-transmitting material containing the pin-hole at the focal plane of the point source(see Fig. 2). This reference wave front then interacts with light passing through the attenuating filter material surrounding the pin-hole, producing interference fringes dependent on the strength of aberration produced by the flow in question.

In a separate and unrelated effort, Anderson and Milton[16] developed an effective way to create a self-aligning spot as part of a study of dark-central-ground interferometry. In their approach, an exposed photographic plate was placed at the focus of the incident beam, and the focused energy of the light source was then used to char the photographic emulsion and thereby create a completely self-aligned point-diffraction spot. Since the point diffractor can be an aperture, or an opaque spot(the resultant wave fronts are mathematically related), this technique offers the same benefits as the Smartt interferometer. Since the mathematical derivations associated with point-diffraction interferometry are well documented in the referenced papers[13-16], the present paper will only address the physical implementation.

3.2 Implementation

In the present application, the primary optics of an existing schlieren system were used[12], with the pulsed Nd:YAG laser replacing the conventional spark as the light source, and a specially created point diffractor replacing the usual knife edge. Figure 3 shows a schematic of the arrangement. The laser light was expanded through a microscope objective to fill the schlieren mirror, transmitted through the test section, and refocused by another schlieren mirror. The exposed photographic plate used to create the point-diffraction spot was placed at the focus of this second mirror, and the laser was pulsed with enough energy to darken, or char the emulsion located at the focal plane of the second mirror. The spot was created *in-situ* by passing light through the test section at a no-flow condition, with the airfoil at 10° angle of attack(the Dark-Central Ground results were quite sensitive to the angle at which the spot was created; the PDI results were not). The spot was precisely tailored to the application under investigation, automatically correcting for nonuniformities

in the light source or optics. The tunnel was turned on and the real-time inteference fringes were recorded on Poloroid film(ASA 3000), and were available for immediate viewing. This was of great value for analysis of the dynamic flow field under investigation, since it permitted rapid review of the progress of the dynamic stall vortex, and on-line retaking of any photograph which was not of the quality required. This also permitted on-line study of the flow field as it developed, since any phase of the cycle could be accessed directly. This ability to actively search for the onset of dynamic stall using the PDI technique is in strong contrast to the more conventional holographic interferometer, which requires a major post-processing effort before the interferogram can even be verified, much less analyzed.

Although this technique is conceptually quite elegant, there were significant implementation difficulties, mostly related to the complexity of the flow field presently under investigation. For example, the PDI technique used light passing through the pin-hole located at the focus of the undisturbed light to create the spherical reference wave front. However, in several cases, particularly at high airfoil angles of attack, most of the flow field was disturbed by the dynamic stall process. This complication led to an investigation of a variety of spot configurations, and ultimately to an exploration of various alternative approaches for generation of the point diffractor. The photographs presented in the present study were obtained using a variation of the PDI technique where the photographic plate was replaced by a blue-line filter. The point diffraction source was then created by burning the filter coating until a *clear* aperture was created on it; this technique resulted in a greatly increased contrast in the interference fringes produced, and permitted full-flow field images to be made with no loss of detail anywhere in the image. The diffraction by the aperture was also insensitive to the angle of the airfoil at which the aperture was produced.

4. Results and Discussion

4.1 Qualitative Analysis of Interferograms

Figure 4a presents a point-diffraction-interferometer image of the NACA 0012 airfoil at 0° angle of attack, in steady flow at M = 0.40. The fringes seen are constant-density contours. The stagnation point is characterized by the convergence of circular fringes which appear at the leading edge. The fringe pattern is symmetrical on both the upper and lower surfaces, indicating the flow is symmetric(appropriate for this airfoil, at 0° angle of attack). The fringes generated at the leading edge terminate on the airfoil surface through an abrupt turning downstream due to the presence of the boundary layer. Since the fringe nearest to the leading edge encloses the stagnation point, correct Mach number values can be assigned to each of the fringes outside of the boundary layer(see Section 5.1).

Figure 4b shows the fringe pattern of an airfoil passing through 10.65° angle of attack, at M=0.40, k=0.05. Note that the circular fringes now appear on the lower surface of the airfoil, reflecting the movement of the stagnation point due to the increase in angle of attack. The concentration of fringes near the leading edge indicates strong acceleration in this region. The fringes originating near the leading edge curve back to the airfoil surface, indicating the presence of adverse pressure gradient on that part of the surface. The presence of the boundary layer can also be seen by the abrupt turning of fringes in the downstream direction as they approach the airfoil surface.

There is a region in the flow near the leading edge which is completely dark in this figure. The very high gradients in this region have so strongly bent the incident light that light from this area is no longer in the field of view by the time its image reaches the image plane(See Fig. 5). Thus, analysis of this region will require re-positioning of the schlieren mirror to a location much closer to the tunnel wall; this arrangement will be used for future study of the details of this critical area.

4.2 Dynamic Stall as Shown by PDI

Figure 6 presents images of the flow field for six angles during the upstroke for M = 0.35, k = 0.05. Figure 6a, taken at 10.65°, is similar to the image discussed above; figure 6b, taken at $\alpha = 12.11°$, shows similar characteristics, indicating that the flow is still attached. Figure 6c shows the character of the flow at $\alpha = 12.54°$. Although the outer flow field remains essentially unchanged, the fringes which rapidly curved back to the surface near the leading edge in figure 6a and 6b no longer do so. Instead, these are now displaced downstream, and show much less curvature until they again come close to the surface, where they abruptly turn normal to the surface. This is the first indication that dynamic stall *delay* (the static stall angle for M=0.35 is 11.6°) has ended, and that the dynamic stall process *itself* has begun. Figure 6d shows this flow for $\alpha = 12.83°$; here, the imprint of the dynamic stall vortex is more clearly delineated. The fringes near the leading edge terminate normal to the surface, and a few of them are curving against the direction of flow, showing the formation of a vortex-like structure. For this case, the outer flow field is still attached. In fact, the outer flow fringes pass smoothly around the dynamic stall vortex, and blend into the boundary layer from 40% chord to the trailing edge.

At $\alpha = 13.85°$, (Fig. 6e), the vortex has moved further down the airfoil, and has grown vertically. Further, although the interference fringes in the downstream part of the vortical region still show contours that might be expected from a classical vortex, the upstream part of the vortical region is much different from that which would be expected from such a vortex. Instead, all the fringes emanate from the leading edge, and enclose a fringe-free region above the airfoil surface. Since this region is vortical in nature, it is not clear that the fringes are still denoting constant velocity contours deep inside this region. It should be noted that the outer flow field was not changed significantly until the dynamic stall induced flow reached the trailing edge of the airfoil(shown in Fig. 6f, $\alpha = 16.02°$). This is in agreement with the lift calculated from integration of instantaneous pressure transducer readings obtained on the surface during related dynamic stall tests[2], which show the lift increasing until the dynamic stall vortex has left the trailing edge.

Although the images shown above were obtained at M = 0.35, the point diffraction technique is not limited to this relatively high Mach number. As can be seen in Fig. 7, the technique produces clear images of the stall process for a wide range of conditions. Figures 7a, 7c, and 7e show

the density field over the airfoil at $\alpha = 10.65^{o}$, k=0.05, for M=0.20, 0.30, and 0.40, respectively. These photographs show the increase in number of density contours that are associated with the increase in speed from M=0.2 to 0.4 as can be seen by comparing these figures to figure 6a, taken at the same angle at M=0.35. Figure 7b, 7d, and 7f show the flow at $\alpha = 14.28^{o}$, after the dynamic stall process has begun, for the same Mach numbers. This clearly shows that the stall vortex occurs earlier in the cycle as the Mach number is increased.

5. Quantitative Analysis of Interferograms

5.1 Determination of Mach Number by Fringe Counting

For a standard interferometer, the path length difference $\overline{\Delta PL}$ due to density (or phase) changes can be related to the fringe number ϵ as,

$$\epsilon = \frac{\overline{\Delta PL}}{\lambda_0} = \frac{1}{\lambda_0}\int (n - n_r)dz$$

For a two-dimensional flow, the above equation can be simplified to,

$$\epsilon = (n - n_r)\frac{L}{\lambda_0}$$

If ϵ is zero or an integer, then the fringe is bright and if it is a half integer, the fringe is dark. Using the Gladstone - Dale equation and the perfect gas equation, the above expression can be reduced to (Goldstein[17])

$$\rho - \rho_r = (\frac{\lambda_0}{n_0 - 1})(\frac{\epsilon\rho_0}{L}) = A\epsilon$$

Since λ_0 = 532 nm, L = 25cm, $(n_0 - 1) = 2.733 \times 10^{-4}$ (from Goldstein[17]), and $\rho_0 = 1.21 kg/m^3$, the constant A can be determined. For the specific case of the present experiments,

$$\rho - \rho_r = 0.009421\epsilon$$

or

$$\frac{\rho}{\rho_0} = \frac{\rho_r}{\rho_0} + \frac{A\epsilon}{\rho_0}$$

Since $\frac{\rho_r}{\rho_0}$ is a function of the free stream Mach number only, $\frac{\rho}{\rho_0}$ can be determined by knowing the fringe number. In this method, a positive fringe number represents deceleration and vice versa.

5.2 Comparison of the Steady and Unsteady Flow Interferograms

Figure 8 presents two interferograms of the airfoil flow at M = 0.3 for an angle of attack of 10.78°. Figure 8a was taken in steady flow; the concentration of fringes near the leading edge shows that the local flow around the leading edge on the upper surface has experienced very strong accelerations as a consequence of the suction that naturally develops at such an angle of attack. The peak local Mach number for this case (corresponding to a fringe number of -14) is $\approx$ 0.61. Also, the airfoil boundary layer thickness at the trailing edge is quite large, of the order of 10% of the airfoil chord. For comparison, Figure 8b shows the flow field for the case where the airfoil passes 10.78° during the upstroke of an oscillation cycle at k=0.05. Although the outer flow does not show much change, the flow near the surface is quite different. For example, only 10 fringes could be detected over it near the leading edge region, corresponding to a peak Mach number of 0.52. It appears that the flow gradients in the unsteady case develop at a slower rate than in the steady case, thus contributing to the delay of stall that is induced by the rapid unsteady motion. Also, the boundary layer thickness at the trailing edge is about half that of the steady case. Eventually, as the airfoil pitches to a higher angle of attack, the unsteady flow gradients attain values that indeed induce flow separation in the unsteady flow as well. The angle of attack at which this condition is reached is a strong function of the Mach number, degree of unsteadiness, amplitude of motion and other parameters. It is expected that further experimentation at a much closer resolution and covering a much broader range of experimental conditions will quantify this comparison. Once separation occurs, the vorticity input by the unsteady motion coelesces into a vortex whose ability to remain on the surface will determine the amount and duration of dynamic lift generation.

5.3. Estimation of Pressure Distribution Around the Leading Edge

As stated earlier, the interferograms represent constant density contours. From these contours, it is possible to compute the Mach number distribution and thus, the pressure distribution around the leading edge. To do this, an interferogram obtained at M = 0.3, k = 0.075 and $\alpha = 12.85^{0}$ was digitized and the region of interest was enlarged. This enlarged image was further 'cleaned up' by digital processing to enhance the contrast and brightness to sharpen the fringes. Because of the appearance of the dark region near the leading edge (see sec. 4. , the definition of the leading edge itself was difficult. To properly define the leading edge, a picture of the airfoil without the flow was obtained, was digitized, and the resulting image was superimposed on the PDI image. The fringes in the PDI image were then extended backwards towards the leading edge, keeping their curvature continuous to intersect the airfoil surface. The Mach numbers for these fringes were computed as explained in sec. 5.2; the corresponding pressure coefficients were calculated and plotted as a function of the distance measured around the leading edge.

Figure 9 presents a portion of the instantaneous local C_p distribution and shows 13 pressure values in a region of 3% chord around the leading edge. The maximum $-C_p$(of 3.8) in the analyzed image occurs at x/c $\approx$ 0.4% for the conditions at which it was obtained. The flow accelerates slowly on the lower surface from the stagnation point and as it passes over the leading edge, the acceleration can be seen to be very rapid. The pressure variation near the leading edge dictates the vorticity production and hence,

its measurement at a fine resolution is critical. Interferometry appears to be the only technique that offers the capability of determining this distribution in such detail. Since it is a non-intrusive method, it offers significant benefits in comparison to other methods such as pressure transducers due to the absence of mechanical interference and the other inherent limitations of mechanical measurement of unsteady pressure(e.g. errors due to dynamic response of the cavities and tubing systems, dynamic calibration etc). Such measurements have been made[2], but the nearest location to the leading edge where the data was obtained in that earlier experiment was still at $x/c = 0.5\%$. To obtain the pressure distribution shown here using the transducers would require an extraordinary number of transducers; the costs concomitant with such a system and the need for a large model to house these and the associated large facility generally preclude such testing.

This result is presented to establish the capabilities of the PDI technique. Many such images are now available, which are being analyzed for quantification of the leading edge flow field so that further understanding of the physics of the flow in this critical region may be obtained.

5.4. Comparison of the Schlieren and PDI Images

Figure 10 compares the flow field pictures obtained with a stroboscopic schlieren technique[7] and the PDI technique. These pictures correspond to nearly identical nominal flow conditions of $M = 0.3$ and $k = 0.075$, at an angle of attack of 14.7^0. The knife edge for the schlieren picture was kept vertical and hence was perpendicular to the streamwise direction. The dark region in Fig. 10a represents an increase in the density gradient towards the knife edge associated with flow deceleration, and hence, the bright regions indicate flow accelerations. The stagnation point can be seen to be at $\approx 2\%$ chord from the leading edge on the pressure side. The same result is seen in Fig 10b, which is a PDI image, wherein the fringes converge towards the stagnation point at the same location. The strongly accelerating flow around the leading edge - the bright region in the schlieren picture - is seen in the PDI image as a large number of fringes (over 20) radiating from the region. The dynamic stall vortex is seen to be at about the 50% chord point in the schlieren picture. This picture also shows that the flow decelerates in the vortex towards the trailing edge. In the interferometry image, the dynamic stall vortex appears as a region with a system of fringes that are nearly concentric on the downstream side of the enclosed region(although they all originate in the leading edge region), and terminate over the airfoil suction side after they turn slightly upstream. A counting of the fringes shows that the PDI image confirms the deceleration of the flow in the vortex towards the trailing edge since the fringe number increases in this direction in the vortex. The two photographs also show a clear demarkation in the edge of the vortical layer. In the PDI image, the vortcial layer is seen to be filled with fringes whose curvature changes to accomodate the local flow conditions. In the schlieren image, this is simply the region where the black and white regions are present. Further downstream of the vortex, there are no significant flow density field changes that can be detected by either of the two techniques.

This strong agreement between the two independently obtained images is noteworthy, even though both are spanwise averaging techniques, use the same flow property - namely density - and also, share some of the optics. The two were obtained on different days, under nominally the same conditions. Despite the changes that could be expected to be present in the instantaneous pictures due to these differences, and from cycle to cycle variations, the two techniques give the same result, with the PDI being also quantitative.

The sharpness of the fringes through the vortical region during the formative stages of the vortex also suggests that the flow through the vortex is nearly two-dimensional. As the vortex grows, it continues to entrain fluid from the outer flow. Near the leading edge, the flow mixes rapidly, and the fringes are lost only in this region, as can be seen in Fig. 7f.

6. Conclusions

Real-time interferometry has now been demonstrated to offer significant benefits for analysis of unsteady compressible flow. In contrast to holographic interferometry, real time techniques permit immediate review and evaluation of the resultant interferograms. This capability is of major value in analysis of dynamic flow fields such as those created by dynamic oscillation of airfoils, and dramatically improves the continuity of analysis of the aerodynamic events; this continuity is critical to improved understanding of dynamic stall.

The interferograms obtained in the present experiment show that the dynamic stall vortex produced by airfoil oscillation in the range of conditions studied to date does not produce the symmetric imprint on the density field that would be expected from a classical vortex. Instead, these images imply that the dynamic stall develops as a region of strong gradients enclosing a region of low energy or weak structure, while still supporting the dynamically modified outer flow associated with the increase of lift that is typical of dynamic stall.

Analysis of interferograms obtained at steady and unsteady conditions show that dynamic motion inhibits the occurrence of the strong suction peaks that appear in steady flow at the same angle of attack. Interferometry permits detailed analysis of these pressure distributions; as many as 13 pressure values have been obtained in the first 1% of the chord, near the leading edge of the airfoil.

Acknowledgements

The project was supported by AFOSR-ISSA-89-0067 and AFOSR-MIPR-90-0012 (monitored by Capt. H. Helin and Dr. L. Sakell) with additional support from NAVAIR (Mr. T. Momiyama) and ARO MIPR-ARO-132-90 (Dr. T.L. Doligalski). We wish to thank Dr. Mark Loomis for introducing us to the dark-central-ground technique. The technical support of Mr. Christopher Boswell of Sterling Federal Systems, Mr. Michael J. Fidrich of the Naval Postgraduate School, and the staff of the NASA Fluid Mechanics Laboratory is greatly appreciated.

7. References

[1] Carr, L.W., "Progress in Analysis and Prediction of Dynamic Stall", *J. of Aircraft*, Vol 25, No. 1, January 1988, pp. 6-17.

[2] McCroskey, W.J., McAlister, K.W., Carr, L.W., Pucci, S.L., Lambert, O., and Indergand, R.F., "Dynamic Stall on Advanced Airfoil Sections", *J. of American Helicopter Society*, July 1981, pp. 40-50.

[3] Carr, L.W., Platzer, M.F., Chandrasekhara, M.S., and Ekaterinaris, J, "Experimental and Computational Studies of Dynamic Stall", *Numerical and Physical Aspects of Aerodynamic Flows IV*, Chapter 14, pp. 239-256, Springer-Verlag, 1990.

[4] Fung, K-Y, and Carr, L.W., "Effects of Compressibility on Dynamic Stall", to be published in *J. of Aircraft*.

[5] Visbal, M. ,"Effect of Compressibility on Dynamic Stall of a Pitching Airfoil", AIAA Paper No. 88-0132, Jan. 1988.

[6] Lorber,P.F., and Carta,F.O., "Airfoil Dynamic Stall at Constant Pitch Rate and High Reynolds Number", *J. of Aircraft*, Vol.25, No.6, pp. 548-556, June 1988.

[7] Chandrasekhara, M.S., and Carr, L.W., "Flow Visualization Studies of the Mach Number Effects on the Dynamic Stall of an Oscillating Airfoil", J. of Aircraft, Vol. 27, No. 6, pp. 516-522, June 1990.

[8] Chandrasekhara, M.S., Carr, L.W., and Ahmed, S., "Comparison of Pitch Rate History on Dynamic Stall", Proc. NASA/AFOSR/ARO *Workshop on Physics of Forced Unsteady Separation*, April 17 - 19, 1990, Moffett Field, CA.

[9] Chandrasekhara, M.S., Carr, L.W., and Ahmed, S., "Schlieren Studies of Compressibility Effects on Dynamic Stall of Airfoils in Transient Pitching Motion", AIAA-90-3038, *Proc. AIAA 8th Applied Aerodynamics Conference*, pp. 346-356, Portland, OR 1990.

[10] Lee, G., Buell, D.A., Licursi, J.P., and Craig, J.E., "Laser Holographic Interferometry for an Unsteady Airfoil Undergoing Dynamic Stall, *AIAA Journal* ,Vol. 22, No.4, April 1984, pp. 504-511.

[11] Jaeschke, M., Hiller, W.J., and Meier, G.E.A., "Acoustic Damping in a Gas Mixture with Suspended Submicroscopic Droplets", *J. of Sound and Vibration*, Vol. 43, No. 3, pp. 467-481, 1975.

[12] Carr, L.W., and Chandrasekhara, M.S., "Design and Development of a Compressible Dynamic Stall Facility", AIAA Paper No. 89-0647, to appear in *J. of Aircraft*.

[13] Smartt, R.N., "Point-Diffraction Interferometry as a Diagnostic for Alignment", *SPIE Vol. 483, "Optical Alignment II"*,1984.

[14] Smartt, R.N., and Steel, W.H., "Theory and Application of Point-Diffraction Interferometers", *J. Appl. Phys.*, Vol 14, Suppl. 14-1, 1975, pp. 351-356.

[15] Bachalo, W.D., and Houser, M.J. , "Evaluation and Application of a New Interferometric Technique for Compressible Flow Research", NASA CR-177467, Oct. 1988.

[16] Anderson, R.C., and Milton, J.E., "A Large Aperture Inexpensive Interferometer for Routine Flow Measurements", *ICIASF'89 RECORD*, IEEE Publication 89CH2762-3, pp. 394-399.

[17] Goldstein, R.J., "Fluid Mechanics Measurements", Chapter 8, Hemisphere Publishing Corporation, 1983.

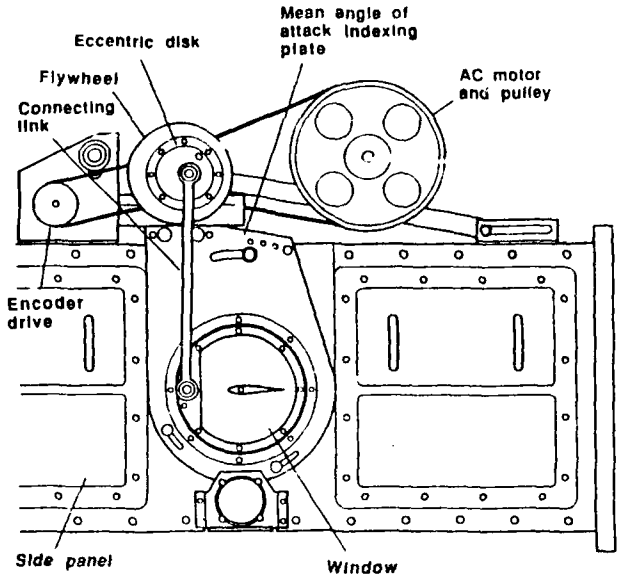

Fig. 1. Schematic of the Compressible Dynamic Stall Facility Test Section.

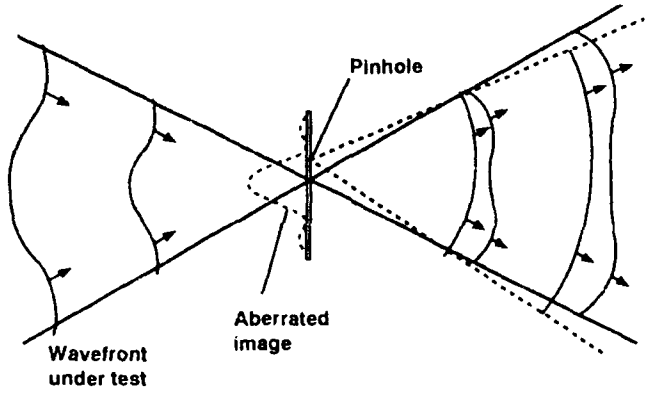

Fig. 2. Schematic of the Principle of Point-Diffraction Interferometry.

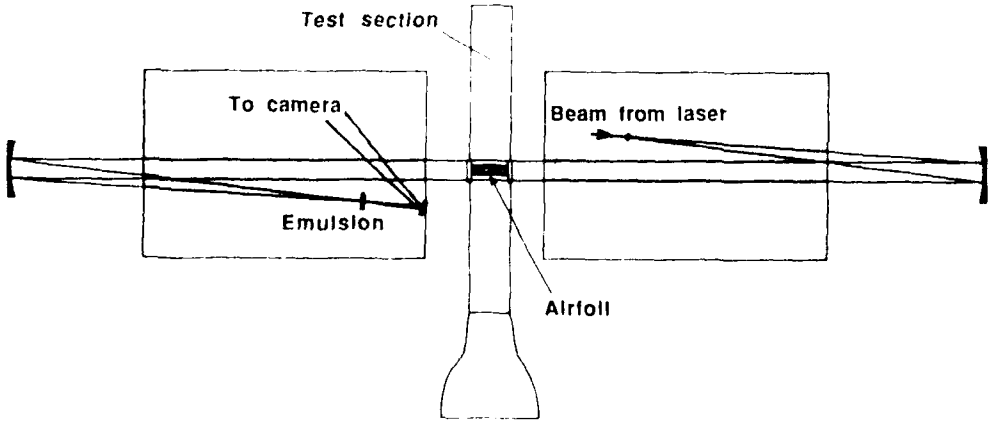

Fig. 3. Schematic of the Layout of Optics for Point-Diffraction Interferometry.

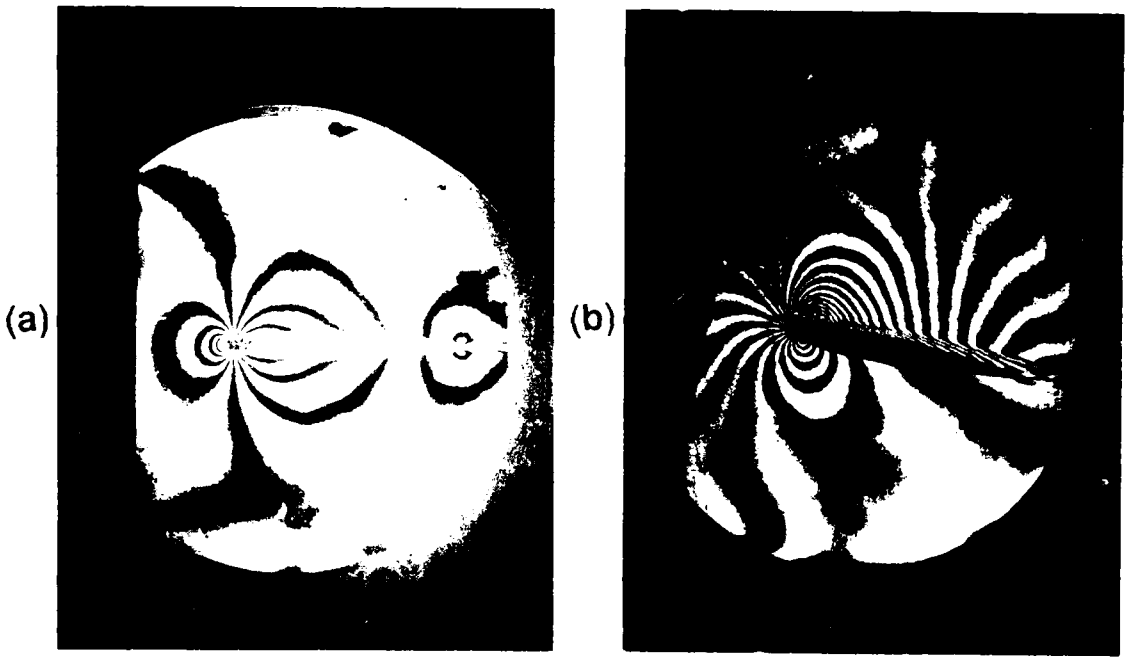

Fig. 4. Representative Interferograms for NACA 0012 airfoil, M = 0.39: (a) α = 0°, k=0.0; (b) α = 10.65°, k=0.05.

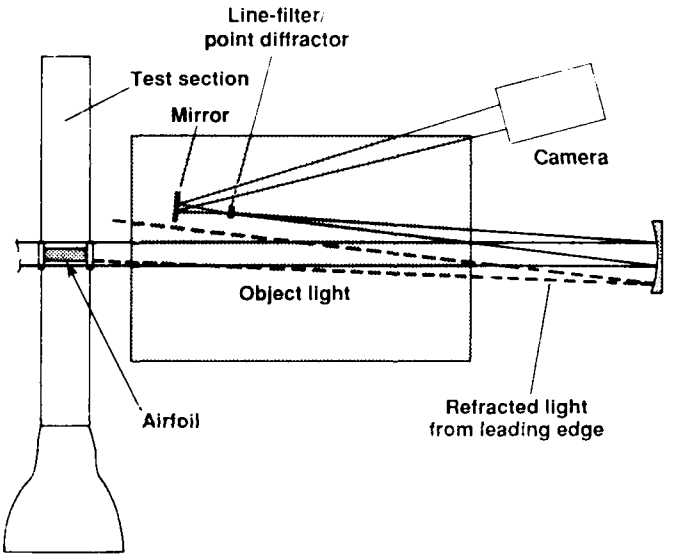

Fig. 5. Effect of Leading Edge Density Gradient on Light Refraction.

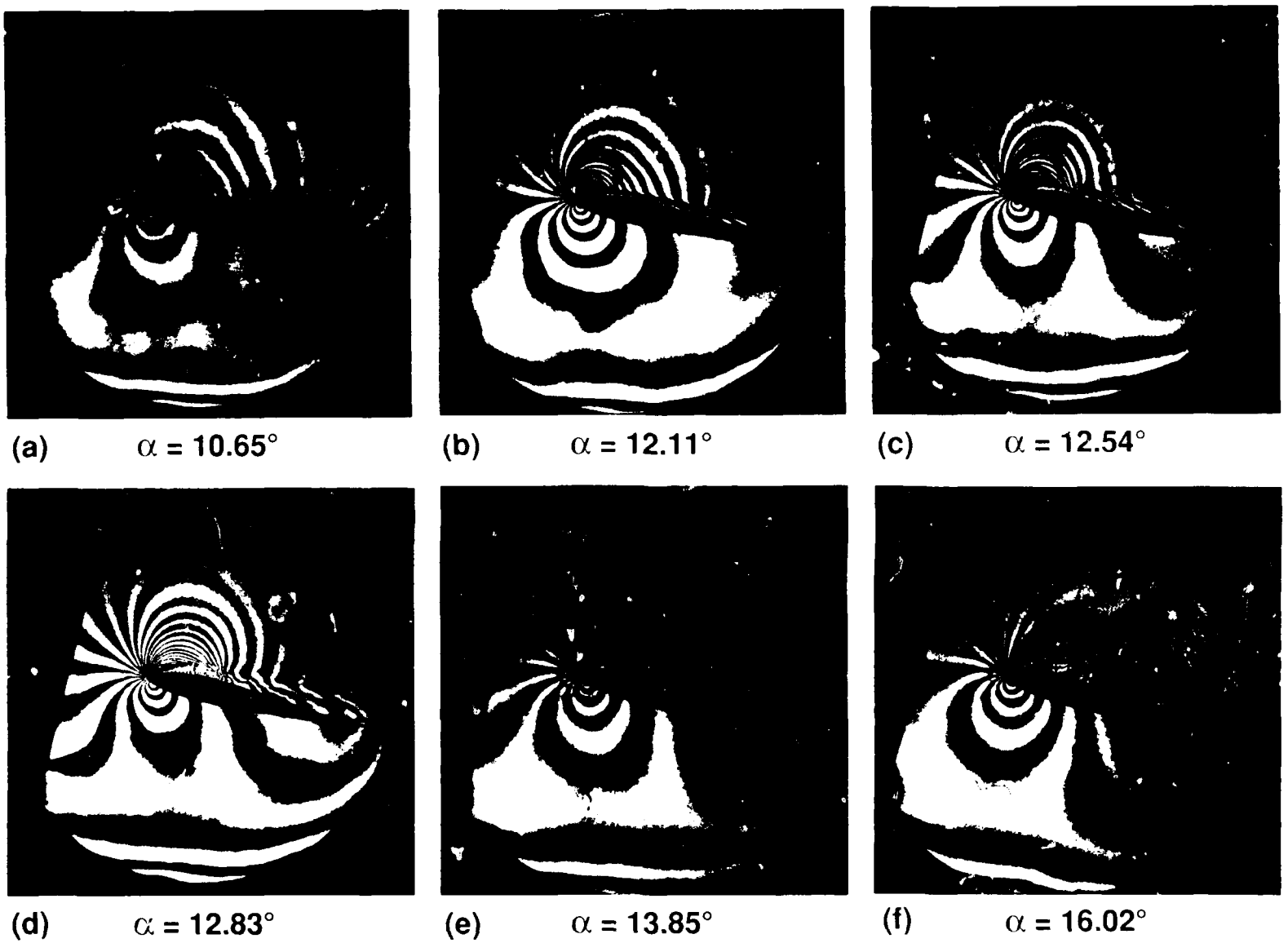

Fig. 6. Sequence of Interferograms Showing Development of Dynamic Stall on an Oscillating Airfoil; M=0.35, k=0.05.

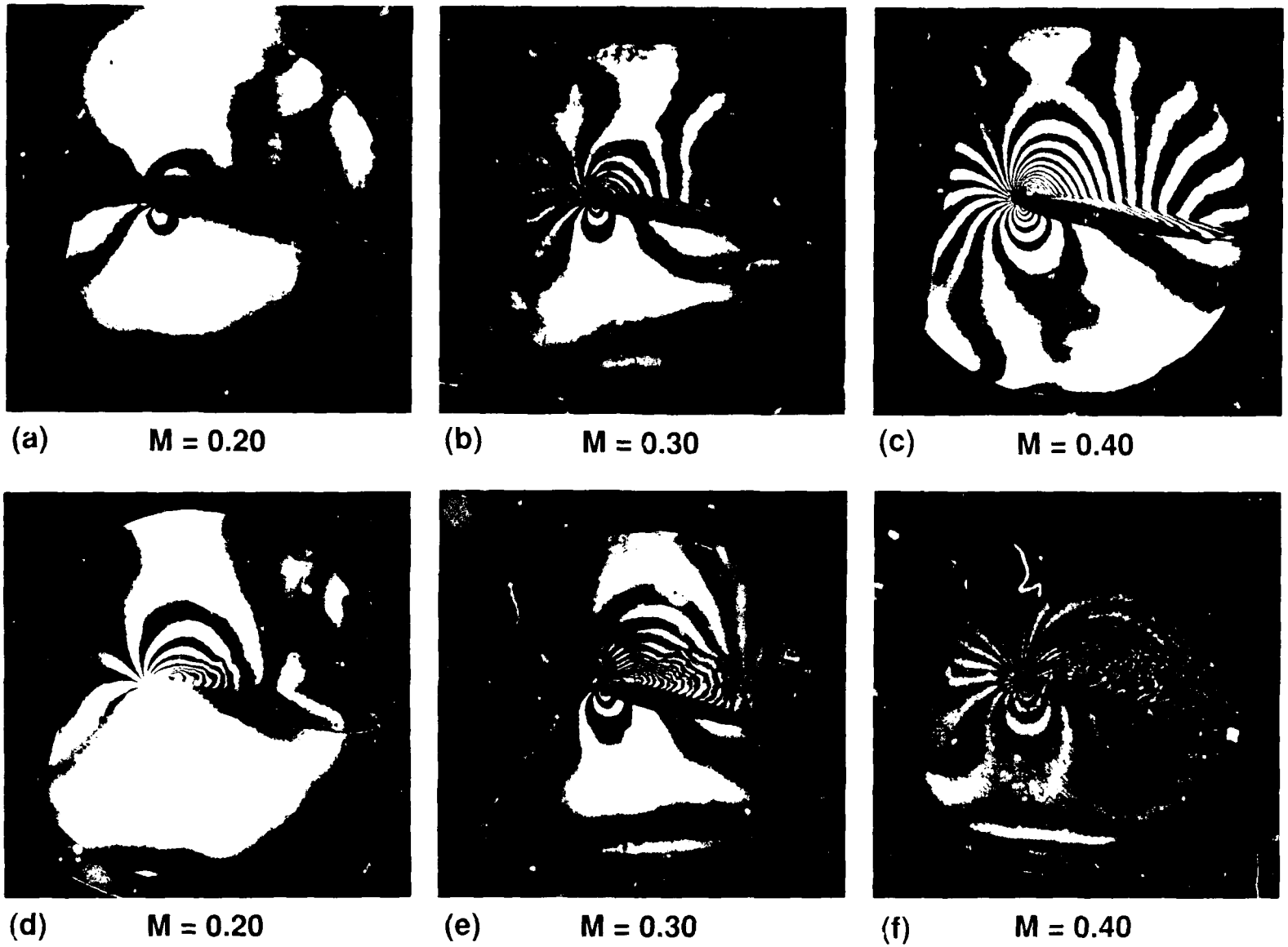

Fig. 7. Interferograms of Oscillating Airfoil Flow at Various Mach Numbers for Conditions Before and During Dynamic Stall; Top Row: $\alpha = 10.65^0$, Bottom Row: $\alpha = 14.28^0$.

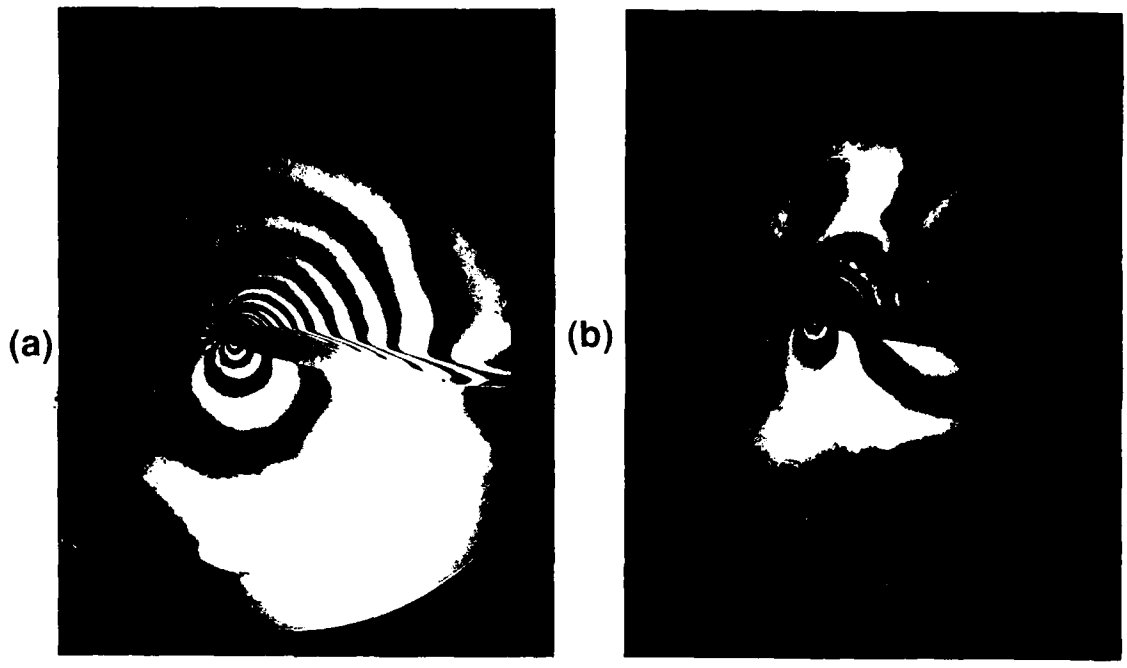

Fig. 8. Effect of Unsteadiness on Flow Field on Airfoil as Shown by Interferometry: M = 0.3, $\alpha = 10.78^0$, (a) k = 0.0, (b) k = 0.05

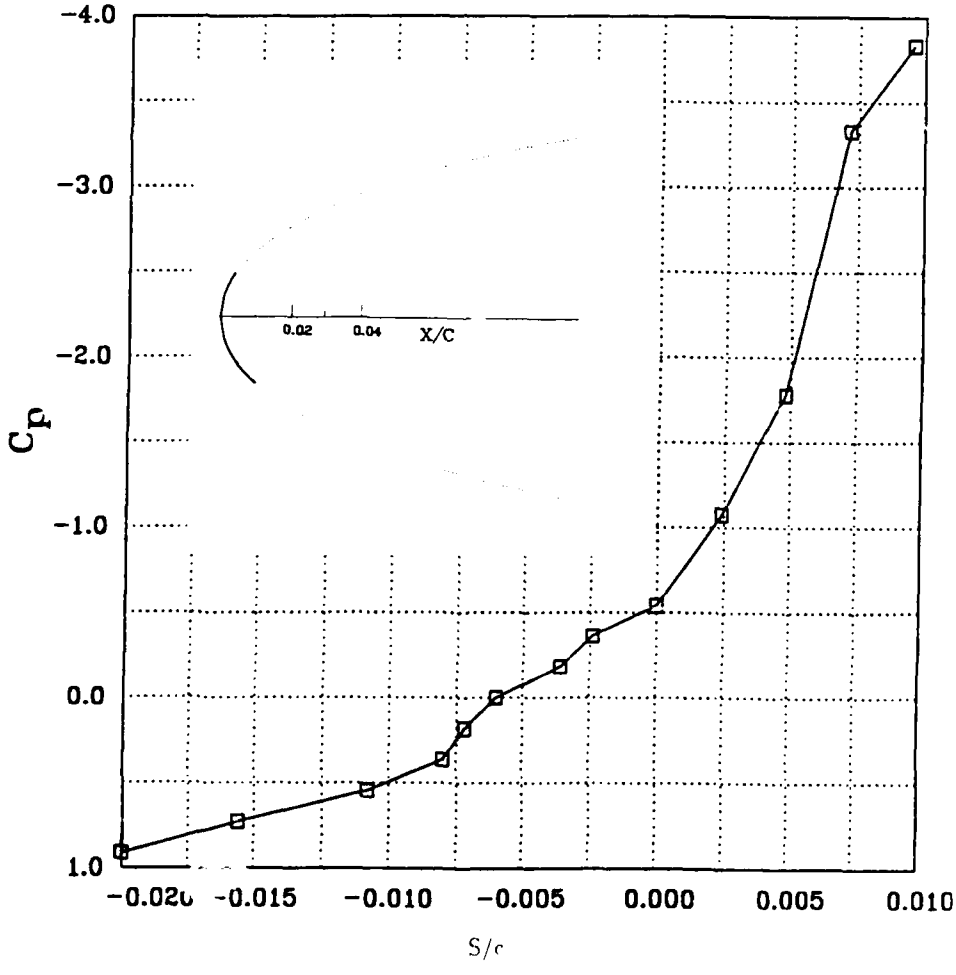

Fig. 9. Pressure Distribution Around the Leading Edge of an Oscillating Airfoil as Determined from Interferogram: M= 0.3, k=0.075, $\alpha = 12.83^0$.

Fig. 10. Comparison of Flow Development Over an Oscillating Airfoil. M=0.3, k=0.075, $\alpha = 14.72°$: (a) Schlieren Picture; (b) Interferogram.